Peer-reviewed version available at *Coatings* **2019**, *9*, 601; doi:10.3390/coatings9100601

Article

Porosity Characterization and Its Effect on Thermal Properties of APS Sprayed Alumina Coatings

Wolfgang Tillmann[1], Omar Khalil [2,*] and Mohamed Abdulagader[2]

[1] Institute of materials science; wolfgang.tillmann@tu-dortmund.de
[2] Institute of materials science; mohamed.abdulgader@tu-dortmund.de
* Correspondence: omar.khalil@tu-dortmund.de; Tel.: (+49-231-755-6113)

Abstract: In the present work, three different atmospheric plasma sprayed (APS) alumina coatings were fabricated using three fused and crushed alumina powders of different particle size fine, medium and coarse. The influence of the particle size on thermal properties and micro-structural features of the produced coating were investigated by thermal insulation test and detailed image analysis technique, respectively. The analyzed micro-structural features include the total porosity, pore size (fine, medium, and large) and cracks. All types of cracks were considered in calculations as voids and were evaluated according to their sizes as pores. All spray parameters except the particle size were fixed throughout the spraying process. The results revealed that the fine starting powder has produced the densest coating with the lowest total porosity and that the total porosity increases with an increasing particle size. This was expected as powders of smaller particle size will reach a higher in-flight temperature and velocity than powders of bigger particle sizes as long as the same spray parameters are applied. However, a detailed image analysis investigation on the three produced coatings showed that the fraction of fine pores and cracks versus the total porosity is substantially higher in coatings produced by using fine starting powders than those produced using medium and coarse powders. In this work, a connection between the thermal insulation and the porosity fraction, which includes fine pores and cracks, was revealed.

Keywords: atmospheric plasma spray (APS) process; particle size; thermal insulation; thermal barrier coating (TBC); thermal diffusivity; coating microstructure; coating porosity.

1. Introduction

Thermal spraying method is a coating process that adds additional thermal and mechanical properties to base substrate materials. In this process, a thick coating is applied to bulk materials substrates which enable them to operate beyond their capabilities in an uncoated state. Ceramics, in general, are particularly suitable for thermal spray processes, with plasma spraying being the most appropriate process due to high temperatures that the plasma jet provides [1]. Atmospheric plasma sprayed (APS) alumina ceramic coatings are very good electrical and thermal insulators. They also improve the resistance of steel against corrosion, wear and erosion. For these reasons, ceramic coatings have been widely investigated [2,3,4,5]. These coatings are being used by the automotive and aerospace industries, where internal components normally operate in severe environments including extreme temperatures [6].During the spraying process, molten alumina particles are heated and accelerated by the plasma jet towards a prepared substrate surface. If these accelerated particles are melted, they impact on the substrate, flattened and form so-called splats. Splats are the main structural unit in APS coatings [1]. The successive deposition overruns define the final thickness and compose the layered structure of the whole coating. In addition to the fully melted particles, APS coatings consist of partially melted particles as well as un-melted particles. The described deposition mechanism leads to a coating with micro structural defects such as pores, delaminations, and micro-cracks. Also, oxide films around the molten particles (droplets), together with un-melted particles, form inclusions in the coating. Fine pores arising from entrapped gas below the molten droplets are

Peer-reviewed version available at Coatings 2019, 9, 601; doi:10.3390/coatings9100601

of spherical shape and homogeneously distributed. The coarse pores, however, are formed due to incomplete filling caused by both semi-molten and un-melted particles and they are non-homogeneously distributed [7]. Oxides, foreign inclusions, as well as un-molten particles are considered to be detrimental to the coating properties; at the same time, the micro-structural features including pores, delaminations, and cracks generated during spraying process improve the thermal insulation of the coating and increase its strain tolerance as well. Hence, the degree of the particle's melting state whilst in-flight affects largely the level of cohesion, porosity, and the ultimate coating's properties [1,8].

Thermal stresses and rapid solidification of in-flight particles are disadvantages related to the APS ceramic coatings. Thermal stresses motivate micro-cracks to initiate and then propagate within the coating, which limits the coating thickness. In a wet environment, micro-structural defects such as pores and cracks may cause local corrosion in the substrate [6], however, the presence of such defects with defined levels enhances the thermal insulation of the coating as well as increases its thermal shock resistance [1]. Un-molten particles exist in the coating when large particles do not have enough time to be fully melted. Only the outer surface of such particles is melted as they impact on the substrate while the inside of the particles is still un-melted [9]. APS alumina coatings have a lamellar microstructure, and defects such as pores and cracks exist generally within/between the lamellae to form an interconnected network. These bi-modular features dramatically influence the mechanical behavior and electrical/thermal insulation of the coating [10,11]. Besides other process parameters, such as the spray power and spray distance, the starting powder particle size has a high influence on the particle's in-flight temperature and velocity. The in-flight particle conditions in turn, determine the particle melting state, impact behavior, and the ultimately produced microstructure of the coating and its properties. [12]. Many researchers have referred to the fact that total porosity plays only a secondary role while the size, shape, and spatial distribution of the pores play the primary role in determining the properties of a coating [13,14].

The present work is based on the study of APS alumina-coating micro-structures using three feedstock powders of different particle sizes that are bonded to steel substrates. The influence of the particle size on the in-flight particle temperature and velocity as well as the coating's microstructural features and the properties of the coating were investigated. The microstructural features of APS alumina coatings including its total porosity, pore area, and crack network were analyzed quantitatively by means of an image processing tool. The work focuses on the accurate measurement of porosity fractions based on a clear criterion that distinguishes each porosity component. Moreover, coating properties such as the micro-hardness and thermal insulation were evaluated and related to the quantified microstructural features.

2. Materials and Methods

2.1 Samples preparation and deposition process:

Three sets of steel substrates with nominal dimensions with a diameter of 40 mm and a thickness of 5 mm were grit blasted using alumina (EFK-14) on one side. This procedure was followed by an ultrasonic cleaning for the APS deposition. Three commercial alumina powders (fused and crushed) of different particle sizes; fine powder, Amperit 740.000 (5-22 μm), medium powder, Amdry 6062 (25-45 μm), and coarse powder, Amperit 740.002 (45-90 μm), H.C.Stark, Germany, were deposited on the steel substrates. The median size (Vol. 50%) of these powders were 14.00 μm, 35.88 μm, and 77.7 μm, respectively.

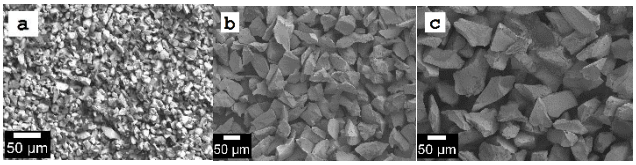

Figure 1. SEM images showing the morphology of the:

Peer-reviewed version available at Coatings 2019, 9, 601; doi:10.3390/coatings9100601

(a)fine, (b)medium, and (c)coarse alumina powders.

SEM images of the utilized powders and their particle size distribution are shown in Figure 1. An Orlikon Metco F4-MB gun, with a nozzle with a 6mm internal diameter and a single powder feeder was used for this study. All spray parameters were kept constant for the three powders in order to investigate the influence of the starting powder's particle size on the microstructural features of the coatings. The APS process parameters are given in Table 1.

Table 1. APS process parameters for alumina powders

Parameter	Value
Current [A]	600
Voltage [V]	74 ± 3
Argon [l.min^{-1}]	41
Hydrogen [l.min-1]	12
Power carrier gas[NLPM]	3.4
Nozzle diameter [mm]	6
Spray distance [mm]	120
Step height[mm]	4

2.2 Porosity Analysis

In order to quantitatively evaluate the porosity of the produced depositions; cross-sectional metallographic samples were prepared for the investigations. A series of SEM images with different magnification factors for each cross-section were taken by a Field Emission Scanning Electron Microscope (Joel, JSM-7001F FESEM). For the porosity measurements, ten images along the cross-section were taken randomly, central to the thickness, for each cross-section. The images were magnified with a magnification factor of 1000x, which enables the detection of 0.1 μm-sized features. The image brightness was reduced while the contrast was increased to facilitate the image analysis software to accurately detect any porosity. Additionally, a very low accelerating voltage (1.0 kV) and a low probe current (8-10 μA) were used so that the contrast between the pores and coating's matrix was enhanced. Additionally, back-scattering electrons feature were used to enhance the quality of the obtained SEM images. An image analysis was performed using the Image J1.49r software (provided by the National Institutes of Health, USA) on SEM images at 1000x. Image filtering was applied to remove noises followed by image segmentation by thresholding, which produced binary images; the zero-threshold level (black) was assigned to the pores and one level (white) to the alumina solid state. Subsequently, the pores were measured and categorized according to three area ranges: Fine (0-1), medium (1-10), and large (>10). Moreover, the medium pore size range (1-10) for the three coatings was further classified in terms of the circularity (cir.<0.5). Circularity is a measuring unit of pore spheroids. The more a pore becomes spherical, the circularity approaches unity and when pores become more elongated or narrow, circularity decreases. Circularity is defined by:

$$4\pi(A/p2), \quad (1)$$

where "A" is the pore area and "p" is the pore perimeter. Various shapes of pores and cracks of different sizes in a cross-sectional SEM image for one coating are identified in Figure 2. The process of pore classification is shown in Figure 3.

Peer-reviewed version available at Coatings 2019, 9, 601; doi:10.3390/coatings9100601

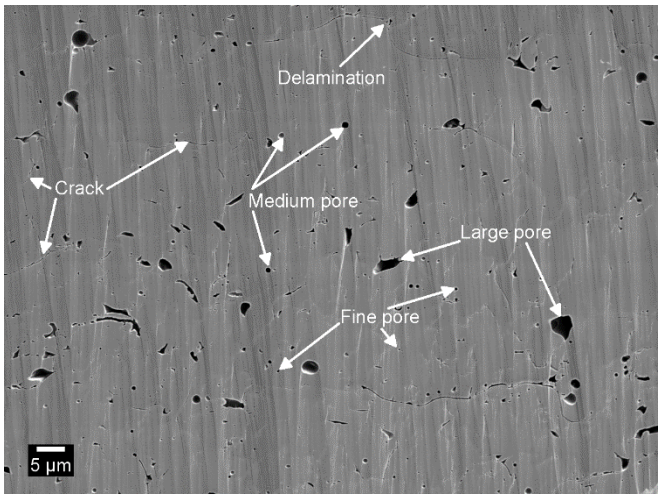

Figure 2. Cross-sectional SEM image showing the shapes and relative sizes of pores and cracks.

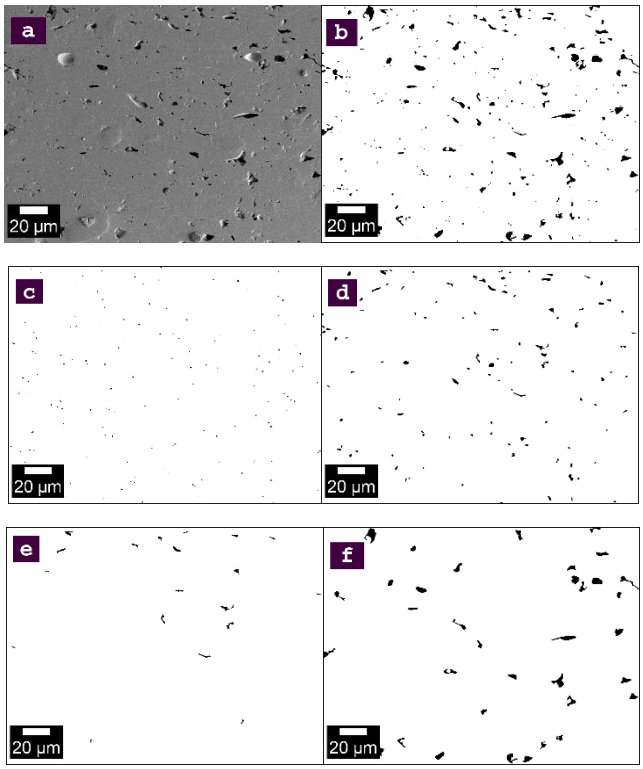

Figure 3. Pore classification process: a) SEM gray image, b) total porosity (binary image), c) fine-pore, d)medium-pore, e) medium-pore with circularity <0.5, f)large-pore class.

2.3 Characterization

A thermal spray sensor (AccuraSpray G3, Tecnar Co., Canada) was used to measure the temperature and velocity of in-flight particles prior the process of samples deposition. The system was positioned so that measurements are taken exactly at the spray distance listed in Table 1.

One sample of each coating was used in the insulation test where the coating surface was subjected to an increasing heat source (oven) up to 900°C with a rate of 15°C per minute, and a holding time of 60 minutes. The temperature on both sides of the three coatings was simultaneously measured by means of two thermocouples. Microhardness measurements were carried out at room temperature on polished cross-sections that represent the three as-sprayed coatings, using a Vickers microindenter (Leco M-400, Germany). The indentations were performed with a load of 2.94 N for a dwell time of 15s. The standard spacing was used between the indentations (at least three times the diagonal) to ensure that no further stresses were produced by the interaction between the consecutive indentations.

Peer-reviewed version available at Coatings 2019, 9, 601; doi:10.3390/coatings9100601

144

145 **3. Results and discussion**

146 **3.1 Image processing analysis**

147 SEM images of as-sprayed coatings were used to analyze the porosity of the produced coatings for
148 the three powders. The porosity level variation in the three coatings is shown in Figure 4. It can be
149 observed that fine pores with an almost spherical shape are uniformly distributed along the coating
150 of the fine-powder. As the particle size increases with medium and coarse powders, more pores of
151 larger sizes are visible and the porosity distribution becomes non-uniform. The image analysis
152 performed on SEM images of coating's cross sections showed that the average total porosity of fine-,
153 medium-, and coarse-powder coatings are 0.93%, 2.47%, and 5.55% of coating area, respectively. In
154 general, the total porosity levels for all coatings increases when increasing the feedstock powder
155 particle size. This increase is mainly due to the simultaneous increase of both the number and size of
156 large pores, whereas fine and medium pores decrease.

157 As all spray parameters were kept constant for the three powders, fine-powder particles were
158 exposed to a higher in-flight temperature and velocity (2620 °C, 415 m/s in average) than medium-
159 and coarse-powder particles (2530 °C, 365 m/s and 2390 °C, 330 m/s in average, respectively). Also,
160 thickness measurements of the three coatings revealed that coarse-powder produce thicker coatings
161 than medium- and fine-powders (avg. thicknesses were 668µm, 475µm and 180µm, respectively).

162 The porosity of the three coatings was evaluated quantitatively and classified into three area ranges.
163 Subsequently, the average porosity of each pore range was calculated. The porosity evaluation was
164 based on ten measurements of ten different SEM images for each coating sample. Given the average
165 pore range porosity and average total porosity for each sample, the percentage of each pore range
166 versus the total porosity was calculated. Additionally, the medium pore range (1-10µm) for each
167 sample was also classified according to the pore's circularity.

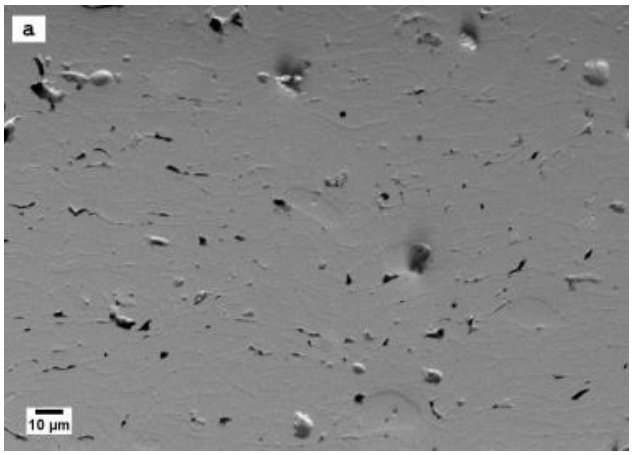

168

Peer-reviewed version available at Coatings 2019, 9, 601; doi:10.3390/coatings9100601

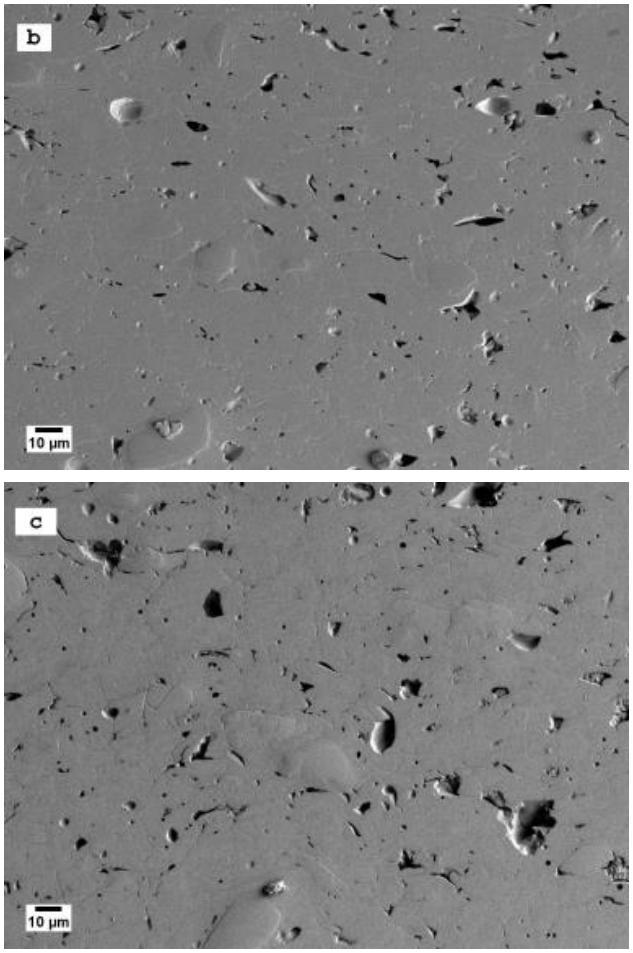

Figure 4. Cross-sectional SEM micrographs of as-sprayed alumina coatings indicating the coating porosity and cracks deposited with: a) fine-powder, b) medium-powder, and c) coarse-powder.

For the medium pore range, the shape of the pores is crucial with regard to the thermal insulation property as pores with a low circularity (circularity < 0.5) highly contribute to the thermal insulation property in comparison to pores with a high circularity (circularity > 0.5). These measurements are visualized in Figure 5. It can be seen that fine-powder coating possesses a higher percentage of fine pores and medium pore ranges (34.4%, 62.3%, respectively) than medium-powder and coarse-powder coatings (15%, 45%, and 6%, 27%, respectively). While more than 60% of the medium pore range for fine-powder coatings exhibit a circularity of <0.5, medium-powder and coarse-powder coatings exhibit less than half (48.2% and 48%, respectively) of medium pore range with the same circularity.

In contrast, coarse-powder coatings possess a higher percentage of large pore ranges (67%) than medium-powder and fine-powder coatings (40% and 3.3%, respectively).

Peer-reviewed version available at Coatings 2019, 9, 601; doi:10.3390/coatings9100601

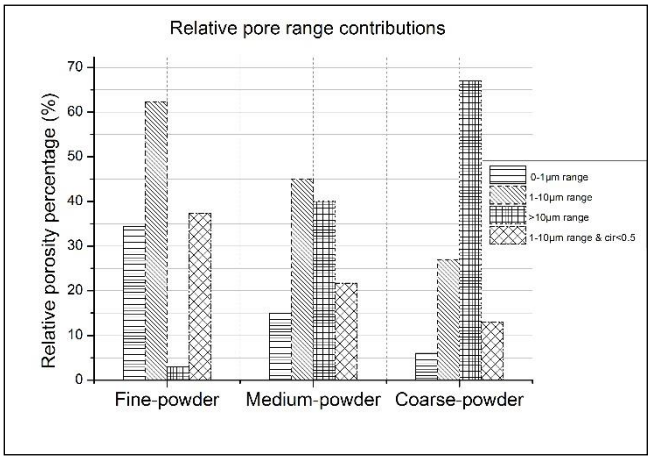

Figure 5. Relative pore range contribution out of total porosity.

3.2 Microhardness

Microhardness tests showed the effect of the coating porosity on microhardness values of the three coatings. Table 2 lists the average microhardness values of the three coatings along with the deviations of these measurements. In comparison to medium- and coarse-powder coatings, fine-powder coatings have the highest microhardness value due to their denser microstructure and lower total porosity. It is noticeable that the deviation value associated with the average microhardness value for the coarse-powder coating is higher than that of the medium- and fine-powder coatings. This can be attributed to the non-uniform distribution of large- and medium-range pores along the coating. In contrast, fine-powder coatings possess the lowest microhardness value due to the relative low pore-size distribution and the very low fraction of large-range pores (3.3%).

Table 2. Average microhardness measurements and associated deviations.

Coating of	Avg. microhardness (HV03)	Deviation
Fine-powder	944	16.2
Medium-powder	881	32.3
Coarse-powder	829	71.4

3.3 Phase Analysis

To justify the different ranges of the pore size distribution in the coatings, the phase composition of the three coatings was investigated and the measurements are given in Figure 6. The three as-sprayed coatings consist of a mixture of α-Al2O3 and γ-Al2O3. However, the main phase was the γ-phase, with the α phase only occurring as a secondary phase. The α-phase is associated with un-molten sprayed powder particles or with molten particles cooled at a low rate. Generally, a high cooling rate leads to a high composition of a γ-phase. The broad, flat area on the curve representing the fine-powder coating (Figure 6-c) indicates that larger amounts of particles were fully molten and their phase changed into a γ phase when compared to medium- and coarse-powders. This implies that a higher fraction of fine-powder particles were fully melted when impacting on the substrate than those in medium- and coarse-powders, which is represented by the γ-phase. Un-molten and partially melted particles of coarse- and medium-powders within the coatings were the source of large pores formations. Therefore, the α-phase, which represents these particles in coarse- and medium-powder coatings (Figure 6-a&b) has a higher level in the composition than that of fine-powder coatings (Figure 6-c).

Peer-reviewed version available at Coatings 2019, 9, 601; doi:10.3390/coatings9100601

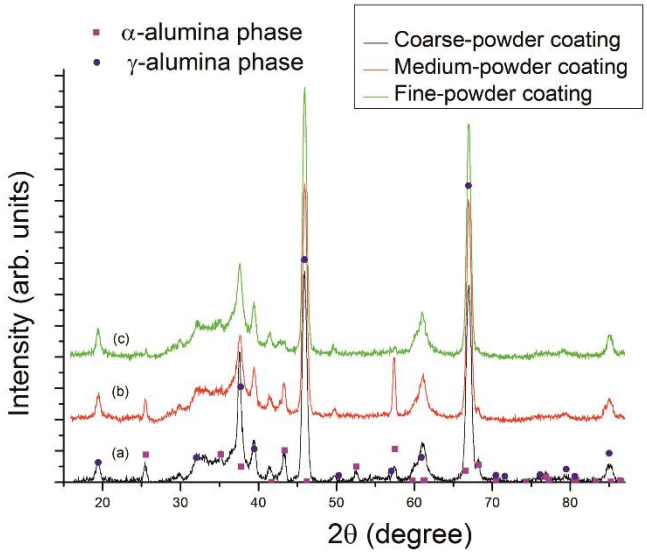

Figure 6. XRD patterns of APS coatings deposited with: a) coarse-powder, b) medium-powder, and c) fine-powder particle sizes.

3.4 Thermal insulation

The thermal insulation of the three coatings is shown in Figure 7. It can be seen that the fine-powder coating possesses a comparable thermal insulation value when compared to the medium- and coarse-powder coatings although its total porosity is much lower (0.93%) than the total porosities of medium- and coarse-powder coatings, (2.47% and 5.55%, respectively). As the porosity of fine-powder coatings consists mainly from pores and cracks of the fine- and medium-range (96.7%), it can be concluded that these ranges of pore sizes and shapes contribute largely to the thermal insulation property and play the primary role in determining thermal insulation value of coatings. The high thermal insulation exhibited by fine-powder coatings can be related to the greater number of interfaces between the pores and the matrix of the coating [14]. Also, the relative high thermal insulation of fine-powder coatings can be related to the higher fine pore density (number of fine pores per unit area), as it can be noticed in SEM images in Figure 4.

Additionally, large pores and medium pores of circularity of >0.5 turn to be of low significance and play only a secondary role in determining the thermal insulation property of coatings, although their presence in medium- and coarse-powder coatings increases greatly the overall porosity.

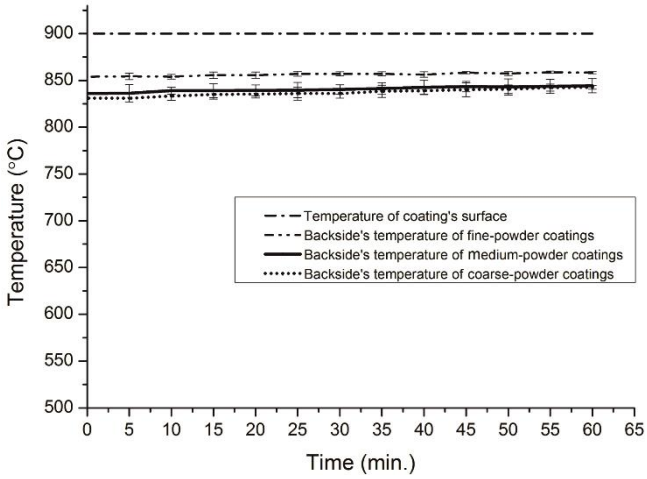

Figure 7. Comparison of thermal insulation of as-sprayed coatings produced by fine, medium, and coarse particle size.

Peer-reviewed version available at Coatings 2019, 9, 601; doi:10.3390/coatings9100601

4 Conclusions

In this study, it was shown that the particle size of the feedstock starting powder has a fundamental effect on the porosity level as well as pore-size distribution, pore shape, and distribution of the overall porosity which highly influence the ultimate thermal coating properties such as the thermal insulation and strain tolerance. According to the obtained results, the following conclusions can be drawn:

1. Coatings produced by fine-powders (i.e. fine particle size) exhibit more uniform pore distribution than coatings produced using medium- and coarse-powders. The pore size ranges from few tenth nanometers to approximately 10um. More than 94% of this range contributes highly to the coating's thermal insulation property due to the uniform distribution, pore size, and pore shape.

2. As the starting powder's particle size increases, the percentage of fine and medium pore ranges (0-1 & 1-10um) versus the total porosity decreases, while the percentage of large pore ranges (>10um) versus the total porosity increases. The increment in large pores greatly increases the total porosity with a low contribution to the coating's thermal insulation.

3. APS coatings fabricated by fine-powders have higher micro hardness values than coatings fabricated by medium- and coarse-powders due to their denser coatings. At the same time, fine-powder coatings exhibit thermal insulation value comparable to thermal insulations of coatings produced by medium- and coarse-powders despite of higher total porosity and coating thichness owned by both medium- and coarse-powder coatings. This is due to the higher contribution of the "effective porosity" in fine-powder coatings represented by fine pores and cracks and to their homogeneous distribution within the coatings.

Author Contributions: supervision, Mohamed Abdulgader; project administration, Wolfgang Tillmann;

Conflicts of Interest: The authors declare no conflict of interest.

References

1. J.R. Davis, Handbook of Thermal Spray Technology, ASM International Materials Park, Las-Vegas, USA, 2009.
2. Pavitra, B., Padture P. and V. Alexandre: Improved interfacial mechanical properties of Al2O3 – 13 wt.% TiO2 plasma-sprayed coatings derived from nanocrystalline powders, ActaMaterialia, Vol. 51 (2003), pp. 2959-2970.
3. Singh, V., Sil, A., and R. Jayaganthan: A study on sliding and erosive wear behavior of atmospheric plasma sprayed conventional and nanostructured alumina coatings, Materials and design, Vol. 32, No. 2 (2011), pp. 584-591.
4. Tingaud,O., Bertrand, P., and G. Bertrand: Microstructure and tribological behavior of Suspension plasma sprayed Al2O3 and Al2O3–YSZ composite coatings, Surface & coating technology, Vol. 205, No. 4 (2010), pp. 1004- 1008.
5. Li, C., Yang, G., and A. Ohmori: Relationship between particle erosion and lamellar microstructure for plasma-sprayed alumina coatings, Wear, Vol. 260, No. 2 (2006), pp. 1166-1172.
6. Morks, M., Cole, I., Corrigan, C., and A. Kobayashi: Electrochemical characterization of plasma sprayed alumina coatings, Journal of surface engineered materials and advanced technology, Vol.1, No.3 (2011)
7. Girolamo, G., Brentari, A., Blasi, C., and E. Serra: Microstructure and mechanical properties of plasma sprayed alumina-based coatings, Ceramic international, 40 (2014).
8. Schlichting, K., Padture, N., and P. Klemens: Thermal conductivity of dense and porous yttria stabilized zirconia, Journal of materials science, vol. 36, No. 12 (2001), pp. 3003–3010.
9. Hurevich, V., Smurov, I., and L. Pawlowski: Theoretical study of the powder behavior of porous particles in a flame during plasma spraying, Surface coatings technology, (2002), pp. 151–152, 370–376.
10. Pawlowski L. et al: The relationship between structure and dielectric properties in plasma sprayed alumina coating, Surface & coatings technology, Vol. 35, (1988), pp. 285-298.

Peer-reviewed version available at Coatings 2019, 9, 601; doi:10.3390/coatings9100601

11. Beauvais, S. et al: Influence of defect orientation on electrical insulating properties of plasma-sprayed alumina coatings, Journal of electroceramics, Vol. 15, (2005), pp. 65-74.
12. Friis, M., Persson, C., and J. Wigren: Influence of particle in-flight characteristics on the microstructure of atmospheric plasma sprayed yttria stabilized ZrO2, Surface coating technology, Vol141, No. 2-3 (2001), p. 115-127
13. Sevostianov,I., and M. Kachanov: Plasma sprayed Ceramic Coatings; Anisotropic elastic and conductive properties in relation to the microstructure; cross-property correlations, Materials science engineering, Vol 297, No.1-2 (2001), pp. 235-243
14. Ravichandran, K., An, K., Dutton, R., and S. Semiatin: Thermal conductivity of plasma-sprayed monolithic and multilayer coatings of alumina and yttria-stabilized zirconia, Ceramic society, Vol 82, No.3 (1999), p.673-682.